

# Quantification of Pinning Center Thickness in Conventionally Processed and Powder Processed Artificial Pinning Center Microstructures

Peter J. Lee and David C. Larbalestier<sup>†</sup>  
Applied Superconductivity Center, University of WI-Madison, Madison WI USA

Paul D. Jablonski  
Teledyne Wah Chang, Albany, OR, USA

**Abstract** — The quantity, size and distribution of pinning centers are key factors in determining the  $J_c$  of Nb-Ti-based superconductors. In Artificial Pinning Center, APC composites large strains must be applied between the assembly of the pinning structure and the final strand, which can result in large changes and variations in pinning center size and shape. In order to correctly interpret the properties of artificial pinning structures, we need an accurate description of their geometry. In this paper we discuss the various techniques available for quantifying near optimum size microstructures and compare the results. We also contrast the distributions found in APC style microstructures with those produced by conventional processing.

## I. INTRODUCTION

By quantifying the microstructure of superconductors we obtain important information that can be used to explain and improve performance. Previously, microstructural studies have shown how cold drawing of conventional Nb-Ti superconductors to peak critical current density produces pinning array dimensions of the order of the coherence length [1] and how this affects the physical properties of the superconductor [2]. They have also shown the direct correlation between volume percent of pinning material and critical current [3] and the pin dimensions and the critical current density versus field slope [4]. In terms of processing we have shown how prestrain influences the precipitate morphology [5],[6] and dimensions [7]. In Nb-Ti-based APC superconductors plane strain deformation of the BCC superconductor matrix results in distortion of the idealized APC arrays towards folded sheet type microstructures that are similar to conventionally processed materials [8]. The deformation of the pinning microstructure is suspected as one of the major contributors to the sometimes disappointing performance of APC superconductors, and yet there is a surprising lack of direct microstructural measurements. The primary reason is the difficulty in preparing transverse cross-sections of the superconducting filaments of high enough quality to provide good contrast between the superconducting and normal phases. However, even when good images are obtained there is still the additional problem of how to quantitatively describe the critical microstructural dimensions. This paper compares a variety of quantification techniques by applying them to conventional and APC microstructures.

Manuscript received October 18, 1994.

<sup>†</sup> also Department of Materials Science and Engineering.

Research supported by the US Department of Energy, Division of High Energy Physics, Grant number DE-FG02-91 ER40643.

## II. EXPERIMENTAL PROCEDURE

The conventional material chosen was a Nb-47.8 wt.%Ti monofilament which was given three precipitation heat treatments of 420C for 288Ks (80h) to give 20 volume % precipitate. This high critical current strand ( $J_c = 3700 \text{ A/mm}^2$ , 5T, 4.2K) has been extensively reported on in previous publications [9],[2]. Transmission electron microscope images of transverse cross-sections were combined to create high atomic number contrast 1024x1024 pixel composite images [10] using a Megavision 1024XM image processor. In all cases manual interpretation of the images was required in order to separate the superconducting and pinning phases accurately into binary images. These monofilaments were fabricated without an external diffusion barrier and Cu diffusion into the Nb-Ti produced a region of smaller precipitates at the outside edge of the foil. For the aggressive heat treatment in this study measurable levels of Cu extend ~10% into the diameter of the filaments [11]. The analyzed areas were taken from the center of the filaments. The binary images used for the conventional composite are shown in Fig. 1.

The APC strand was fabricated by powder processing and warm hydrostatic extrusion [12], [13] using 20 volume % of Nb pinning material in a 55 wt.% matrix. Micrographs of transverse cross-sections, at strains of 3.22 to 7.23 from assembly, were obtained by Backscatter Electron Spectroscopy on a JEOL 35C Scanning Electron Microscope. Binary images derived from those micrographs are shown in Fig. 2.

In these highly cold drawn superconductors the microstructures extend uniformly over the sampling depth of both imaging techniques, allowing the use of random transverse cross-sections to represent the microstructural distribution.

The binary images were quantified using both the Megavision system and a Microsoft Windows based analysis program, Mocha by Jandel Software.

## III. RESULTS

### A. Precipitate Thickness by Direct Measurement

1) *Minimum distance at intercept:* In this technique measurement points are selected on a feature in a random [1] or ordered [14] manner and the minimum thickness of the feature measured at that point. Here we use concentric circles similar to those used in ASTM grain size measurements in order to select feature positions. This technique produces a measurement which is close to what we intuitively think of as a thickness and, provided enough measurements are made, provides an estimate of the variability in thickness within a

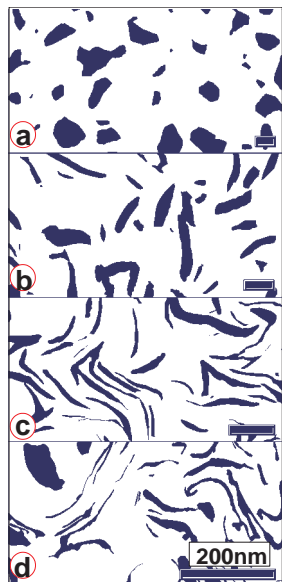


Fig. 1. Details from the binary images of the conventionally processed Nb-Ti series,  $\alpha$ -Ti in black, (a) after final heat treatment,  $\epsilon_f=0$ , (b)  $\epsilon_f=1.11$ , (c)  $\epsilon_f=2.50$ , and (d)  $\epsilon_f=3.98$ . Scale bar = 200nm.

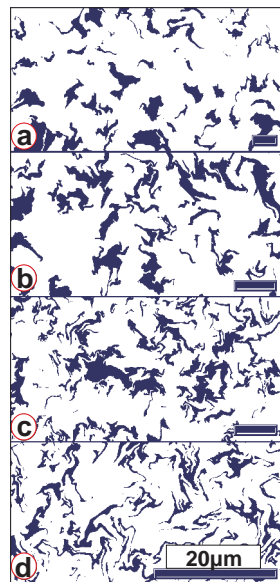


Fig. 2. Details from the binary images of the powder processed APC composite at strains of a) 3.22, b) 4.47, c) 5.08 and d) 7.23 after initial assembly. Scale bar = 20 $\mu$ m.

given cross-section. It does, however, become increasingly arbitrary as the measured objects become more irregular. An approach which is more applicable to irregular shaped objects is to measure *the length through the particle of a line perpendicular to a tangent fitted to the intersected surface*. For parallel ribbons this produces a similar result to the “minimum distance” approach providing compatibility with older reported measurements. It is this definition we use in this study. Although it should be possible to automate this technique, at present we are forced to determine these thicknesses manually.

Frequency graphs for the conventional material at a final strain of 2.50 are shown in Fig. 3. (a) using linear bin intervals and (b) logarithmic intervals. Clearly the logarithmic distribution is a better model than the linear. We find this to be the case for *all* our measurements in this study. However, we will give analyses based on both normal and log-normal statistics. The results for both the conventionally processed monofilament and the APC composite are shown in Table I.

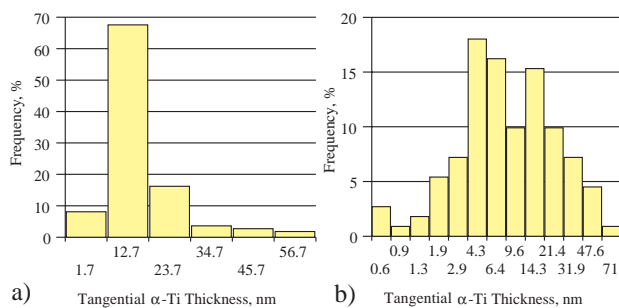


Fig. 3. Frequency histograms for tangential  $\alpha$ -Ti thickness measurements for the conventionally processed monofilament,  $\epsilon_f=3.98$ , using a) linear and b) logarithmic bin intervals.

TABLE I  
THICKNESS BY CIRCLE SELECTED MINIMUM (TANGENTIAL) METHOD

Final Strain $\epsilon_f$	Normal, nm		Log-Normal, nm					
	Mean	$\sigma_{n-1}$	Mean	Mean	Mean	Mean	Mean	Coeff. of Var. %*
			$-2\sigma_{n-1}$	$-\sigma_{n-1}$		$+\sigma_{n-1}$	$+2\sigma_{n-1}$	
$\alpha$ -Ti Thickness for the Conventionally Processed Monofilament								
0	<b>147.6</b>	53.3	29.0	59.7	<b>122.9</b>	253.1	66.1	106
1.11	<b>55.3</b>	52.9	10.2	21.0	<b>43.4</b>	89.8	185.8	107
2.50	<b>18.7</b>	11.9	3.3	7.0	<b>14.9</b>	31.3	66.1	111
3.98	<b>10.2</b>	10.4	0.9	2.4	<b>6.4</b>	17.3	46.7	170
Nb Thickness for the Powder Processed APC								
3.22	<b>4209</b>	4497	194	666	<b>2288</b>	7864	27027	244
4.47	<b>2247</b>	2438	157	465	<b>1371</b>	4047	11943	195
5.08	<b>1528</b>	1939	130	349	<b>936</b>	2507	6714	168
7.23	<b>388</b>	471	26	76	<b>223</b>	651	1902	192

\* Calculated from the Mean value minus the Mean+ $\sigma_{n-1}$  value

In both cases the average values of thickness derived from log-normal statistics are much smaller than from normal statistics. The distribution of particle thicknesses in the APC composite are typically twice as broad as for the conventional strand.

2) *Minor Axis*: An automated technique for the direct measurement of particle width is Minor Axis measurement. Firstly the Major Axis is determined from the two points on a particle's edge that are furthestmost apart. The distance between these points is called the Major Axis Length (the Major Axis being a straight line connecting those two points). The Minor Axis thickness is defined as the length of the longest line perpendicular to the Major Axis that can be drawn through the particle.

The results of these analyses are shown in Table II. The results are similar to the tangential thickness measurements for the simpler shapes of the low strain conventional material but give increasingly exaggerated values as the shapes become more complex, as in the high strain conventional ribbon

TABLE II  
MINOR AXES

Final Strain $\epsilon_f$	Normal, nm		Log-Normal, nm					
	Mean	$\sigma_{n-1}$	Mean	Mean	Mean	Mean	Mean	Coeff. of Var. %*
			$-2\sigma_{n-1}$	$-\sigma_{n-1}$		$+\sigma_{n-1}$	$+2\sigma_{n-1}$	
$\alpha$ -Ti Thickness for the Conventionally Processed Monofilament								
0	<b>151.1</b>	110.4	22.1	50.0	<b>113.4</b>	256.9	582.0	126
1.11	<b>59.5</b>	40.0	6.7	17.1	<b>43.9</b>	112.5	288.2	156
2.50	<b>31.2</b>	38.1	1.4	4.8	<b>16.7</b>	57.6	199.1	245
3.98	<b>20.8</b>	23.5	0.8	2.9	<b>10.9</b>	40.4	149.4	271
Nb Thickness for the Powder Processed APC								
3.22	<b>10611</b>	9577	542	1861	<b>6395</b>	21974	75501	244
4.47	<b>6431</b>	7428	100	520	<b>2689</b>	13909	71947	417
5.08	<b>4349</b>	5285	127	516	<b>2093</b>	8487	34413	305
7.23	<b>703</b>	1248	11	48.8	<b>224</b>	1027	4706	358

\* Calculated from the Mean value minus the Mean+ $\sigma_{n-1}$  value

microstructures and the APC composites.

3) *Random straight line intercept distance*: We introduce this automated measurement as having a useful application to superconducting microstructures. This is a measure of the distance traversed across an object by a random straight line. In a truly random microstructure (as these transverse cross-sections tend to be) parallel lines can be chosen. Consequently it can be used to interpret the behavior with respect to a rigid fluxon lattice. For aligned microstructures, lines can be used that are perpendicular to the alignment axis. For these random microstructures, we use a large number of vertical and horizontal lines to maximize the pixel resolution of the digital technique. Using this technique, a large amount of data can be obtained from the microstructure without user interaction. The results of this approach are shown in Table III, where values typically 30% greater than those obtained by minimum (tangential) intercept are reported.

### B. Indirect Methods

These methods calculate the average thickness of individual particles from other measured dimensions. They require complete features for accuracy and give frequency rather than volume weighted statistics. In general volume weighted statistics, i.e., random line intercepts, are more useful in explaining the physical properties, whereas frequency weighted data are more useful for interpreting composite deformation behavior. A comparison of the data generated by these techniques is given in Table IV.

1) *Feret Diameter*: This is the simplest of the indirect measurements, the “diameter,”  $d^*$ , being calculated from the cross-sectional area of the particle,  $A$ , as

$$d^* = 2\sqrt{(A / \pi)} , \quad (1)$$

by assuming the particle to be circular. Although this is really a diameter rather than a thickness measurement, it is included here for comparison as it is often used to describe the initial

TABLE III  
STRAIGHT LINE INTERCEPT THICKNESS

Final Strain $\epsilon_f$	Normal Statistics, nm		Log Normal Statistics, nm			
	Mean	$\sigma_{n-1}$	Mean	Mean	Mean	Coeff. of Var. %*
			$-\sigma_{n-1}$		$+\sigma_{n-1}$	
$\alpha$ -Ti Thickness for the Conventionally Processed Monofilament						
0	<b>164.1</b>	107.2	55.7	<b>126.0</b>	285.0	126.2
1.11	<b>76.0</b>	61.7	23.8	<b>55.9</b>	131.3	134.9
2.50	<b>28.3</b>	26.6	8.7	<b>20.3</b>	47.4	133.5
3.98	<b>14.3</b>	14.2	3.7	<b>9.5</b>	24.1	153.7
Nb Thickness for the Powder Processed APC						
3.22	<b>4563</b>	5049	646	<b>2345</b>	8518	262.9
4.47	<b>2690</b>	2713	548	<b>1641</b>	4911	199.1
5.08	<b>1961</b>	2225	446	<b>1221</b>	3346	174.0
7.23	<b>494</b>	524	107	<b>304</b>	860	182.9

\* Calculated from the Mean value minus the Mean+ $\sigma_{n-1}$  value

TABLE IV  
INDIRECT THICKNESS MEASUREMENTS

Final Strain $\epsilon_f$	Model	Normal, nm		Log Normal, nm		
		Mean	$\sigma_{n-1}$	Mean	Mean	Coeff. of Var. %*
				$-\sigma_{n-1}$	$+\sigma_{n-1}$	
$\alpha$ -Ti Thickness for the Conventionally Processed Monofilament						
0	Feret Diameter, $d^*$	<b>179.1</b>	112.6	70.0	<b>143.4</b>	104.8
	Rectangle Quadratic	<b>103.7</b>	61.5	41.5	<b>84.1</b>	102.9
	Modified Rectangle	<b>93.0</b>	53.7	39.6	<b>77.0</b>	94.2
	Skeletal	<b>87.2</b>	70.0	26.1	<b>62.3</b>	138.4
1.11	Feret Diameter, $d^*$	<b>100.3</b>	59.2	41.1	<b>82.1</b>	99.6
	Rectangle Quadratic	<b>40.9</b>	22.8	17.6	<b>34.1</b>	93.6
	Modified Rectangle	<b>38.2</b>	21.1	16.9	<b>32.1</b>	90.0
	Skeletal	<b>46.6</b>	29.2	19.1	<b>38.0</b>	98.4
2.50	Feret Diameter, $d^*$	<b>56.3</b>	38.2	21.4	<b>44.4</b>	107.7
	Rectangle Quadratic	<b>13.8</b>	7.7	5.9	<b>11.5</b>	93.9
	Modified Rectangle	<b>13.4</b>	7.5	5.7	<b>11.1</b>	94.6
	Skeletal	<b>15.8</b>	12.5	5.8	<b>12.2</b>	111.5
3.98	Feret Diameter, $d^*$	<b>32.3</b>	23.7	11.8	<b>25.0</b>	111.2
	Rectangle Quadratic	<b>7.6</b>	8.7	2.7	<b>5.6</b>	107.1
	Modified Rectangle	<b>7.3</b>	7.9	2.7	<b>5.5</b>	103.6
	Skeletal	<b>10.6</b>	16.5	2.4	<b>6.1</b>	154.1
Nb Thickness for the Powder Processed APC						
3.22	Feret Diameter, $d^*$	<b>9946</b>	6947	3118	<b>7350</b>	135.6
	Rectangle Quadratic	<b>1908</b>	1329	612	<b>1423</b>	132.4
	Modified Rectangle	<b>1880</b>	1304	605	<b>1403</b>	132.1
4.47	Feret Diameter, $d^*$	<b>6192</b>	5084	1265	<b>3886</b>	206.7
	Rectangle Quadratic	<b>1053</b>	687	304	<b>768</b>	152.3
	Modified Rectangle	<b>1040</b>	681	299	<b>757</b>	153.4
5.08	Feret Diameter, $d^*$	<b>4332</b>	4027	1212	<b>2980</b>	146.3
	Rectangle Quadratic	<b>721</b>	390	328	<b>610</b>	85.7
	Modified Rectangle	<b>717</b>	385	329	<b>608</b>	84.9
7.23	Feret Diameter, $d^*$	<b>805</b>	979	166	<b>465</b>	179.6
	Rectangle Quadratic	<b>150</b>	115	52	<b>113</b>	115.1
	Modified Rectangle	<b>147</b>	114	51	<b>110</b>	115.5

\* Calculated from the Mean value minus the Mean+ $\sigma_{n-1}$  value

non-deformed microstructures.

2) *Thickness By Rectangular and Rounded End Rectangle Models*: The average thicknesses,  $T$ , of more complex shapes is better calculated from the area and perimeter,  $P$ , of the particle using the quadratic solution for a rectangle

$$T = P/4 - 1/\sqrt{(P^2 - 16A)} . \quad (2)$$

A more complex model adds semi-circular ends to the rectangle to approach a more realistic shape:

$$T = 1/\pi(P - \sqrt{(P^2 - 4\pi A)}) . \quad (3)$$

The results of the quadratic formulae are very similar for the complex shapes found in these superconductors. The values are slightly lower than minimum (tangential) intercept values because the undulations in the particle surfaces are not taken into account.

4) *Skeletal thickness*: The particles are digitally eroded to pixel width to form a skeleton; the average thickness is obtained by dividing the cross-sectional area by the length of the skeleton.

For ribbon-like microstructures, the values generated by this technique are very similar to those obtained by direct measurement by the minimum (tangential) intercept approach.

#### IV. DISCUSSION

A. The APC microstructure is quite different to the conventionally processed material. The APC Nb pins deform in a jagged irregular manner compared with the precipitated  $\alpha$ -Ti. Likely reasons are:

A.I. The impact of the plain strain deformation of the  $\beta$ -Nb-Ti matrix on the HCP  $\alpha$ -Ti is much less than the combined interaction of the two APC BCC phases.

A.II. The  $\alpha$ -Ti precipitates are mono-crystalline and because they are precipitated at  $\beta$ -Nb-Ti triple points are neighbored on each surface by single BCC grains. This contrasts with the polycrystalline pins of the APC where many grains interact to distort the pins.

B. The jagged deformation of the APC is reflected in the broad distribution in pin dimensions shown in Tables I-III (direct measurements) which indicate a size range which is 50% to 100% larger than for the conventional composites.

C. The indirect measurements (Table IV) on individual features, however, give a similar width for the distribution of individual pin sizes for both conventional and APC microstructures. The range is fairly constant (in terms of percentage) with strain. This indicates that the microstructure of the APC is stable over this strain range.

D. The largest change in dimensions with strain was found when the conventionally processed material was cold drawn from the relatively equiaxed heat treated condition to the ribbon morphology. We have observed similar behavior in the initial deformation of APC composites. Once the ribbon microstructure is developed, the deformation is more uniform.

#### E. Recommended Measurements:

E.I. *The random straight line technique*: This method provides thicknesses that have a physical significance in terms of flux pinning and proximity coupling behavior. It is fast and easy to apply to pin separation as well as thickness. The values obtained for ribbon microstructure are slightly higher than previously obtained by minimum value techniques.

E.II. *The quadratic-rectangle model*: This provides an easy to apply method of describing the average thickness of individual particles and is useful in describing the deformation of the pin lattice. It appears to slightly underestimate the dimensions of complex pin shapes.

#### V. CONCLUSIONS

1. The method used to obtain particle thickness from the same micrograph can influence the result substantially.
2. Extrapolations of microstructural dimensions are questionable unless backed up by measurements.
3. It is important to report a measurement that accurately describes the microstructure. We recommend more than one type of measurement: Firstly a direct volume measurement such as *random linear intercept distance* to aid in the interpretation of physical properties. Secondly a shape model to describe individual particle deformation.
4. The correct statistical model (in these cases the log-normal distribution function) must be used to describe the particle size distribution.
5. Utilizing the appropriate measurements we can usefully contrast the APC microstructures with those of conventional superconductors.

#### REFERENCES

- [1] P. J. Lee and D. C. Larbalestier, "Development of nanometer scale structures in composites of Nb-Ti and their effect on the superconducting critical current density," *Acta. Met.*, vol. 35, pp. 2526-2536, 1987.
- [2] C. Meingast, P. J. Lee and D. C. Larbalestier, "Quantitative description of a high  $J_c$  Nb-Ti superconductor during its final optimization strain: I. Microstructure,  $T_c$ ,  $H_{c2}$  and resistivity," *J. Appl. Phys.*, vol. 66, pp. 5962-5970, 1989.
- [3] P. J. Lee, J. C. McKinnell, and D. C. Larbalestier, "Restricted Novel Heat Treatments for Obtaining High  $J_c$  in Nb-46.5wt%Ti," *Adv. Cryo. Eng.*, vol. 36, pp. 287-294, 1990.
- [4] P. J. Lee and D.C. Larbalestier, "An examination of the properties of SSC Phase II R&D strands," *IEEE Transactions on Applied Superconductivity*, vol. 3, pp. 833-841, 1993.
- [5] M. I. Buckett and D. C. Larbalestier, "Precipitation at low strains in Nb46.5wt%Ti," *IEEE Trans. Mag.*, vol. 23, pp. 1638-1641, 1987.
- [6] P. J. Lee, J. C. McKinnell, D. C. Larbalestier, "Progress in the Understanding and Manipulation of Microstructure in High  $J_c$  Nb-Ti Alloy Composites," Proc. of New Developments in Applied Superconductivity, ed. Y. Murakami, World Scientific Press, 1989, pp. 357-362.
- [7] P. J. Lee, J. C. McKinnell, and D. C. Larbalestier, "Restricted Novel Heat Treatments for Obtaining High  $J_c$  in Nb-46.5wt%Ti: II. Prestrain Dependence," *Adv. Cryo. Eng.*, vol. 40A, pp. 725-732, 1994.
- [8] L. D. Cooley, P. J. Lee and D. C. Larbalestier, "Is Magnetic Pinning a Dominant Mechanism in Nb-Ti?," *IEEE Trans MAG*, vol 27, pp. 1096-1100, 1991.
- [9] Li Chengren and D. C. Larbalestier, "Development of high critical current densities in Niobium 46.5wt% Titanium," *Cryogenics*, vol. 27, pp. 171-177, 1987.
- [10] P. J. Lee, "Enhancement of atomic number contrast for image analysis of highly strained materials," *Proc. of EMSA*, vol. 45, pp. 358-359, 1987.
- [11] K. J. Faase, W. H. Warnes, P. J. Lee and D. C. Larbalestier, "Microstructural and Compositional Gradients in the Filament-Matrix Region of Nb-Ti Wire Composites," presented at the Applied Superconductivity Conference, Boston, MA 1994, submitted for publication in *IEEE Trans. Applied Superconductivity*, October 1994.
- [12] P.D. Jablonski and D.C. Larbalestier, "Niobium-Titanium superconductors produced by powder metallurgy having artificial flux pinning centers," *U.S. patent*, no. 5,226,947, July 13, 1993.
- [13] P. D. Jablonski, P. J. Lee and D. C. Larbalestier, Development and Characterization of Artificial Microstructures in Long Lengths of Superconducting Wire," *Mat. Res. Soc. Symp. Proc.*, vol. 351, pp. 455-457, 1994.
- [14] J. M. Seuntjens, F. Y. Clark, T. J. Headley, A. C. Kilgo and N. Y. C. Yang, "Quantification of second phase morphology in SSCL VQP samples," *Adv. Cryo. Eng.*, vol. 40, pp. 793-798, 1994.